ARTICLE

Spin Polarized Conductance in Hybrid Graphene Nanoribbons Using 5−7 Defects

Andrés R. Botello-Méndez,[†] Eduardo Cruz-Silva,[‡] Florentino López-Urías,[†] Bobby G. Sumpter,[‡] Vincent Meunier,[‡] Mauricio Terrones,[†,*] and Humberto Terrones[†]

[†]Laboratory for Nanoscience and Nanotechnology Research (LINAN) & Advanced Materials Department, IPICYT, Camino a la Presa San José, 2055, San Luis Potosí 78216, Mexico, and [‡]Oak Ridge National Laboratory, P.O. Box 2008, Oak Ridge, Tennessee 37831-6367

ABSTRACT We present a class of intramolecular graphene heterojunctions and use first-principles density functional calculations to describe their electronic, magnetic, and transport properties. The hybrid graphene and hybrid graphene nanoribbons have both armchair and zigzag features that are separated by an interface made up of pentagonal and heptagonal carbon rings. Contrary to conventional graphene sheets, the computed electronic density of states indicates that all hybrid graphene and nanoribbon systems are metallic. Hybrid nanoribbons are found to exhibit a remarkable width-dependent magnetic behavior and behave as spin polarized conductors.

KEYWORDS: graphene · nanoribbons · magnetism · quantum transport · half metallicity · *ab initio*

The ability of synthesizing single layers of graphite (referred to as graphene) with large surface areas (up to cm^2) has opened a new exciting area of research.[1,2] These 2D materials possess unique electronic properties that arise from an unusual linear band dispersion (for a comprehensive review of the electronic properties of graphene, see ref 3). Size effects play a particularly important role in graphene materials. Depending on the shape of the edges, graphene nanoribbons could present different electronic properties. For instance, zigzag nanoribbons exhibit edge states that are not present in the armchair case.[3−6] These edge shapes have been observed experimentally and are found to be stable for over micrometer sizes.[7] Recently, it has been demonstrated that graphene can be cut selectively to form zigzag and armchair nanoribbons.[8,9] Such developments have prompted investigations toward using these materials in devices such as p−n and p−n−p junctions, which are essential in electronics.[10,11]

Numerous theoretical studies have focused on tailoring the electronic properties of graphene and graphene nanoribbons for nanoelectronics applications. Some researchers have adopted an approach similar to that of conventional semiconductor industry and focused on ion impurities and vacancies (doping).[12,13] Others have incorporated adsorbed molecules or ions at the edges or studied the effect of different substrates. Another promising approach consists of joining an armchair and a zigzag nanoribbon by rotating the cutting direction, resulting in Z-shaped,[14−17] T-shaped,[18,19] L-shaped,[20,21] cross-shaped,[22−24] and arrow-shaped[25−27] graphene nanoribbon intramolecular junctions.

For any graphene-based application to be viable, it is essential to understand the effect of defects and disorder. In this context, it is known that edge roughness strongly affects the electronic and transport properties of graphene nanoribbons.[28]

Here, we present results obtained for nanoribbon junctions that are based on an ordered array of structural defects. Such arrays of defects have been observed experimentally and could be visualized as grain boundaries in a graphene or graphite crystal.[29] In particular, an array of pentagons and heptagons can be used to join an armchair and a zigzag nanoribbon. Andriotis and Menon have used a similar approach to construct T-junctions with all zigzag or armchair edges and compute junction transport properties as a function of the size of the branches.[18,30] In this work, we present a complete study on the electronic and magnetic properties of 2D hybrid armchair−zigzag graphene and 1D hybrid armchair−zigzag graphene nanoribbon systems using density functional theory (DFT), as well as the electron transport for the 1D structures. We find that 2D hybrid graphene sheets have states at the Fermi level and that hybrid nanoribbons exhibit spin polarized transport as well

*Address correspondence to mterrones@ipicyt.edu.mx.

Received for review June 10, 2009 and accepted October 16, 2009.

Published online October 28, 2009.
10.1021/nn900614x CCC: $40.75

as unusual magnetic properties that depend on the width of the zigzag section.

RESULTS AND DISCUSSION

Geometry of Grain Boundaries in Graphene. In 1992, Terrones and Mackay proposed that graphene can exhibit grain boundaries by the inclusion of pentagons and heptagons, preserving the total Gaussian curvature equal to zero at the graphene layer and changing the chirality in such a way that zigzag and armchair edges coexist in the same structure (see Figure 1).[31] This kind of grain boundary was studied before[32] and has been observed experimentally by scanning tunneling microscopy (STM) in highly ordered pyrolytic graphite (HOPG).[29] In addition, it has been shown that these kinds of defects could be easily identified experimentally with IR and Raman spectroscopies.[33] A whole new class of finite graphene structures (nanoribbons) could be built following the main idea outlined in the study of graphitic grain boundaries. When simulating the diffraction pattern of graphene with a 5−7 grain boundary, we find that zigzag and armchair features are present in the form of a pattern with 12 spots (see Figure 1c). Such fingerprint could be useful for experimentally identifying these systems.

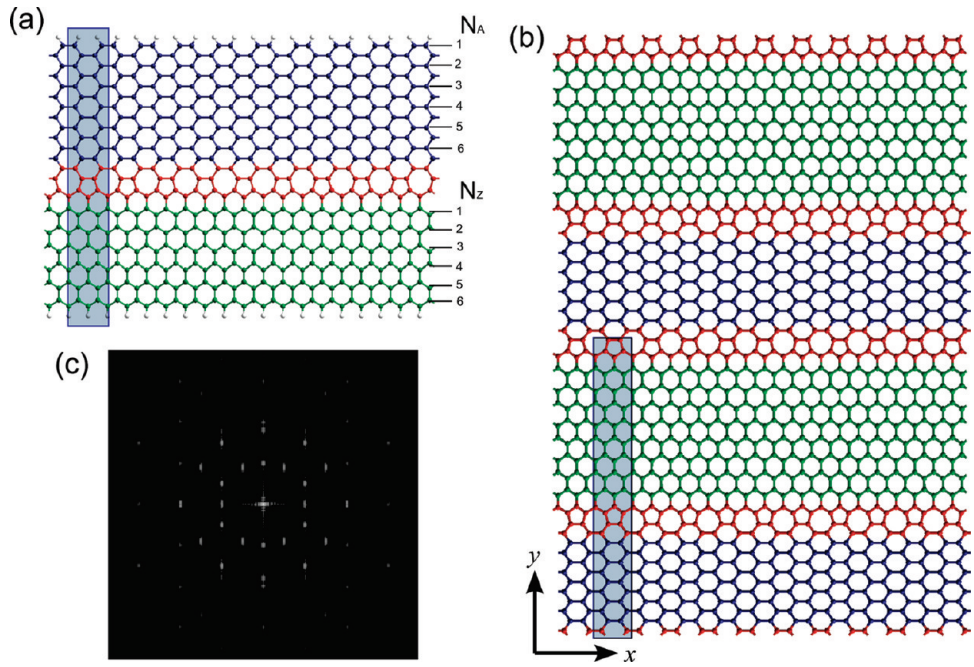

Figure 1. Molecular models of ordered arrays of pentagon−heptagon defects on (a) a hybrid graphene nanoribbon ($N_A = N_Z = 6$) and (b) a $N_A = 5$, $N_Z = 8$ single hybrid graphene layer. The shaded region represents the unit cell for each case; the nanoribbon is periodic on the *x* direction, while the graphene layer is periodic in *x* and *y*. Colors indicate the armchair (blue), zigzag (green), and 5−7 chain region (red) for clarity. (c) Simulated diffraction pattern of graphene with a 5−7 grain boundary.

In this work, we have used a linear array of pentagons and heptagons as a grain boundary to rotate a piece of a graphene, and in this way, smoothly converting an armchair nanoribbon into a zigzag nanoribbon (see Figure 1a). In other words, an armchair nanoribbon (blue part in Figure 1) can be joined to a zigzag nanoribbon (green part in Figure 1) using a grain boundary formed by a linear array of pentagons and heptagons (called 5−7 chain from here on), thus forming a hybrid nanoribbon (HNR). Similarly, a 2D system can be constructed by merging zigzag and armchair ribbons consecutively (Figure 1b), thus creating a hybrid graphene (HG). Different systems could be constructed in a systematic way by tweaking the number of armchair dimers (N_A) and the number of zigzag chains (N_Z), resulting in a (N_A,N_Z) HNR or a (N_A,N_Z) HG for the 1D and 2D cases, respectively. Additionally, more complex 1D systems could be achieved by incorporating more than one 5−7 chain, thus resulting in armchair(N_A)−zigzag(N_Z)−armchair(N_A) HNRs or zigzag(N_Z)−armchair(N_A)−zigzag(N_Z) HNRs, and so on.

The incommensurability of the graphene ribbons in the zigzag and armchair directions is manifest in these structures. The armchair segments are under

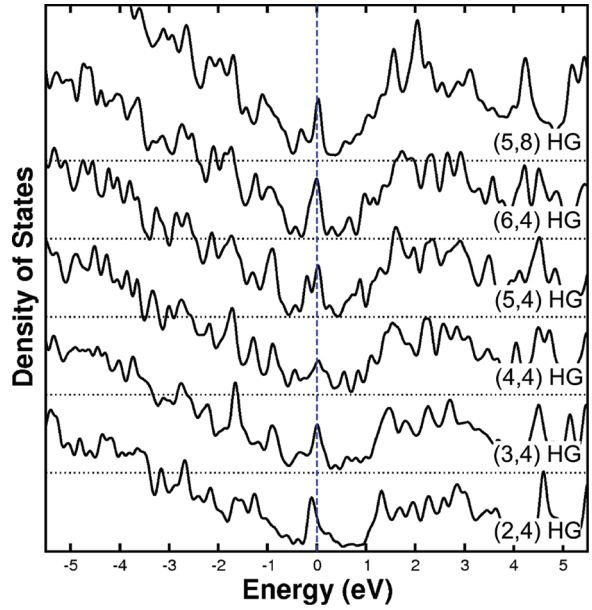

Figure 2. Electronic density of states for hybrid graphene layers with different armchair widths. Note that all of the systems exhibit a large density of states around the Fermi level (E_F is set to zero). When the number of armchair dimers N_A is a multiple of 3, there is an increment on the states at the Fermi level.

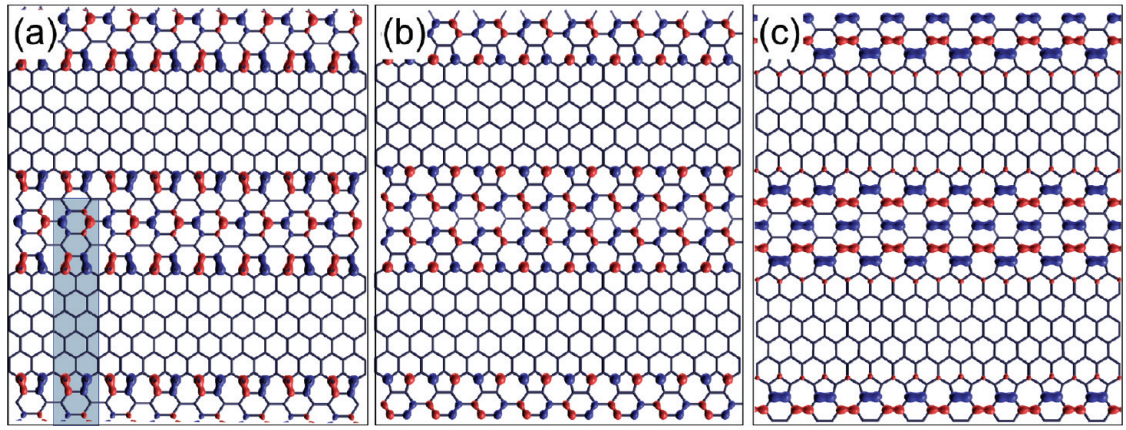

Figure 3. Wave functions with energies (E) around the Fermi level plotted at gamma point: (a) −1.2, (b) −0.2, and (c) 0.12 eV. The shaded region in (a) represents the unit cell of the (3,4) hybrid graphene layer.

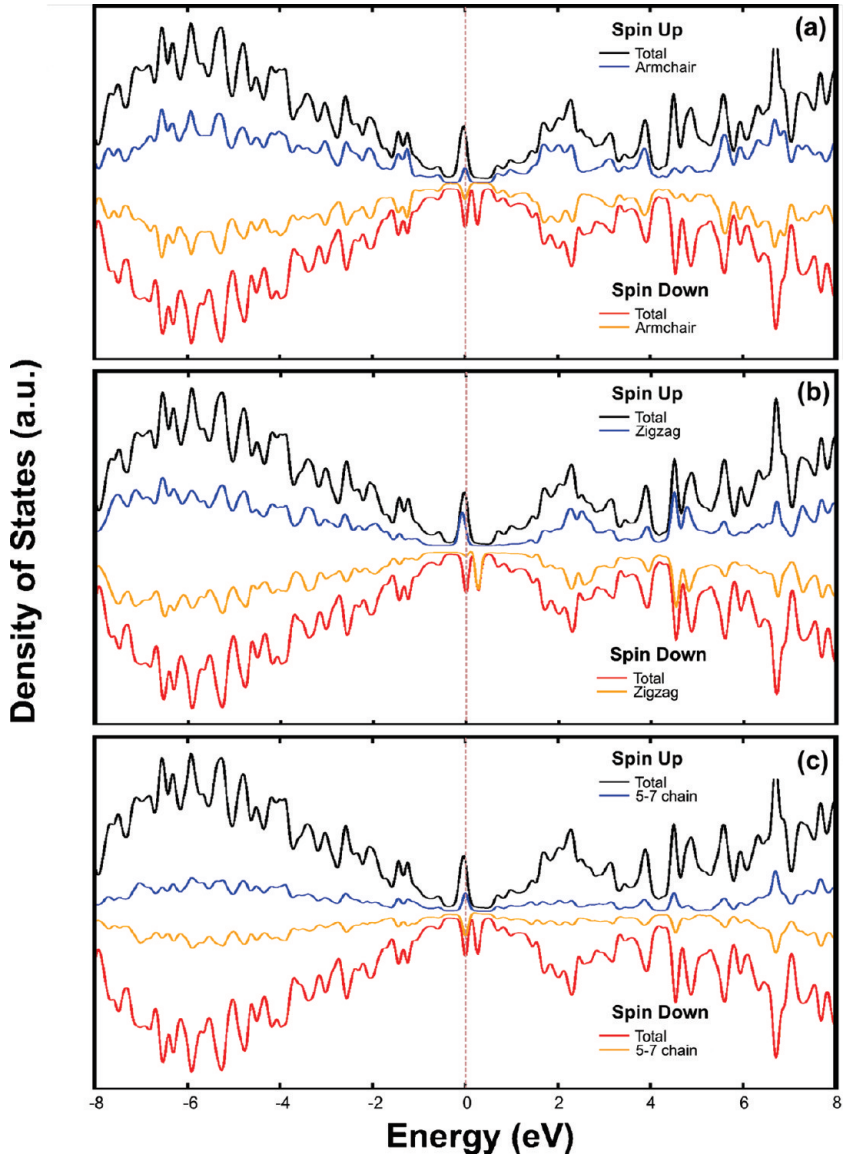

Figure 4. Spin resolved total DOS compared to the local DOS on the (a) armchair, (b) zigzag, and (c) 5−7 chain regions of a (4,4) hybrid nanoribbon. Note that all regions contribute to the states near the Fermi level (E_F = 0); however, only the zigzag region contributes to the magnetic moment.

tension, whereas the zigzag segments are under compression. The hexagonal network is deformed, and the angles change from 120 to 114.7, 122.6, and 122.6° for the armchair case and 113.6, 123.2, and 123.2° for the zigzag case. The bond lengths are also distorted, being extended up to 1.54 Å for the armchair section and compressed up to 1.38 Å in the zigzag case.

Electronic and Magnetic Properties. It is well-established that the electronic properties of armchair ribbons depend on their width, resulting in three families of nanoribbons. In particular, ribbons with $N_A = 3p$, where p is an integer, are semimetallic, according to LDA calculations,[34] or have a small band gap in calculations including electron−electron interactions.[35] In any case, it is interesting to investigate the effect of width on the electronic properties of the hybrid graphene systems described above.

Two-Dimensional Hybrid Graphene. We have computed the electronic properties of HG with different armchair and zigzag widths. In particular, we have studied (2,4)−(6,4) HG and (5,8) HG systems. Despite the different widths, all of the systems show similar behavior. In close similitude to the related Haeckelites systems, all of the 2D systems show states at the Fermi level (E_F).[36] The density of states (DOS) of these systems is shown in Figure 2. LSDA calculations revealed a zero magnetic moment. It is important to note that some of the states around the E_F could be induced by symmetry loss due to lattice distortion.

In order to further investigate the properties of the states lying close to the

Fermi energy, we represent isosurface contour plots of three wave functions with energies around the Fermi level (see Figure 3). The states close to E_F are localized at the interface between the nanoribbon regions and the 5−7 chain. The first wave function plotted (Figure 3a) exhibits states at the zigzag region edges hybridized with states at the pentagons of the 5−7 chain. In addition, some states in the middle of the armchair region are present. The second wave function (Figure 3b) shows the typical zigzag edge states found in zigzag nanoribbons. States along the armchair region similar to those found in armchair nanoribbons are also observed. Finally, the third wave function (Figure 3c) shows states at the armchair region closely related to the conduction bands of armchair nanoribbons. We can conclude from these observations that the general effect of the grain boundary is to shift down the Fermi level of the armchair nanoribbons in order to achieve band alignment.

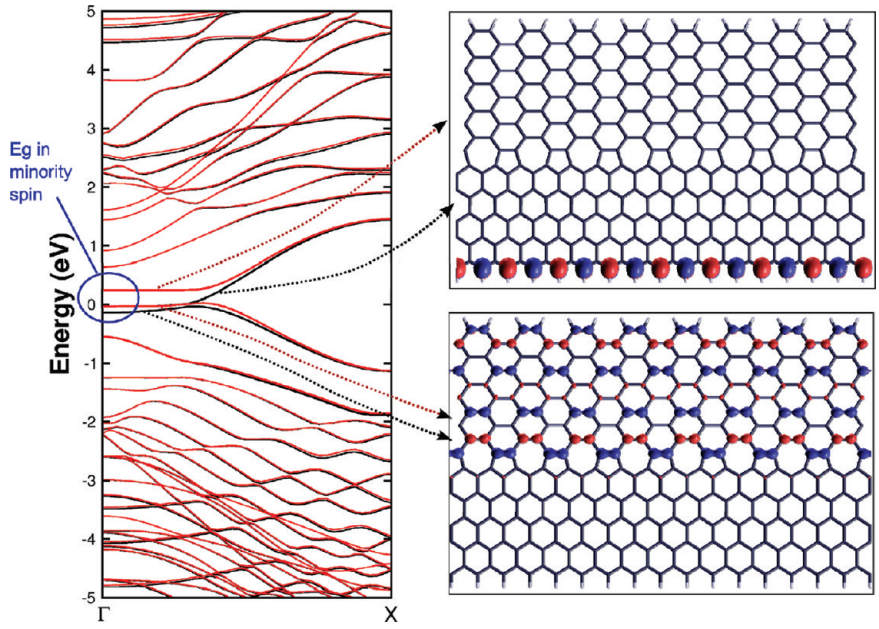

Figure 5. Left: Computed spin polarized band structure for a (4,4) hybrid nanoribbon. Note the energy gap (E_g = 0.27 eV) on the minority spin (red). The arrows illustrate the region of the HNR that contributes to the bands marked. Right panels show the wave functions of the bands close to the Fermi level plotted at the gamma point.

Hybrid Nanoribbons. Our calculations show that HNRs could exhibit unusual electronic and magnetic properties. It can be observed that HNRs are degenerate in most of the energy spectrum, with the exception of the region close to the Fermi level. The spin resolved DOS for a (4,4) HNR shown in Figure 4 exhibits states at the Fermi level and a magnetic moment $\mu = 0.35\ \mu_B$. Figure 4a−c shows the total DOS compared to the local DOS projected on the armchair, zigzag, and 5−7 chain regions, respectively. This detailed analysis indicates that the three regions of the HNR contribute to the states at the Fermi level. However, only the zigzag region contributes to the magnetic moment, which is consistent with previous nanoribbon calculations using only zigzag architectures.

The spin resolved band structure for a (4,4) HNR is shown in Figure 5 left. It can be noted that there is a small energy gap of *ca.* 0.2 eV in the minority spin states. Table 1 shows that, for ribbons with an even width, there is a gap in the spin down states; that is, the systems exhibit half metallicity (spin polarized conduction). We confirmed the presence of this energy gap obtained within the local spin density approximation by using the Perdew−Burke−Ernzerhof functional within the spin polarized generalized gradient approximation (s-GGA) for the hybrid nanoribbons obtaining similar results, which are summarized in Figure S1 in the Supporting Information. In addition, the calculation of the (4,4) hybrid nanoribbon using the hybrid PBE0 functional for exact exchange shows an energy gap of the minority spin at the Γ point.

The isosurface plots of the wave functions close to the Fermi level are represented in right panels of Figure 5. It can be noted that some of these bands (top) are closely related to the zigzag nanoribbon edge states. However, it is important to note that, opposite to a zigzag nanoribbon, there is only one edge state. It has been previously found that, for zigzag nanoribbons, an antiferromagnetic configuration between ferromagnetically ordered edge states at each edge is energetically favored over the configuration with same spin orientation between the two edges,[37] thus resulting in a null total magnetic moment. However, in this case, since there is only one ferromagnetically ordered edge state, there is always a net magnetic moment.

We have constructed more complicated zigzag−armchair−zigzag HNRs. In this case, there are two zigzag edge states, but they are separated by an armchair segment and two 5−7 chains. When the armchair segment width is small, there is interaction between the ferromagnetically ordered edges (*e.g.*, in the

TABLE 1. Dependence of the Electronic and Magnetic Properties on the Width of the Armchair and Zigzag Regions in HNRs

system	magnetic moment (μ_B) LSDA	spin down E_g(eV) LSDA	magnetic moment (μB) s-GGA	spin down E_g (eV) s-GGA
(3,3) HNR	0.27	0.00	0.20	0.04
(4,4) HNR	0.35	0.27	−0.42	0.42
(5,5) HNR	0.02	0.00	−0.43	0.36
(6,6) HNR	0.43	0.22	−0.45	0.34[a]
$N_Z = 8, N_A = 5, N_Z = 8$	0.00	0.00		
$N_Z = 3, N_A = 8, N_Z = 3$	0.54	0.00		

[a]Energy gap present in majority carriers.

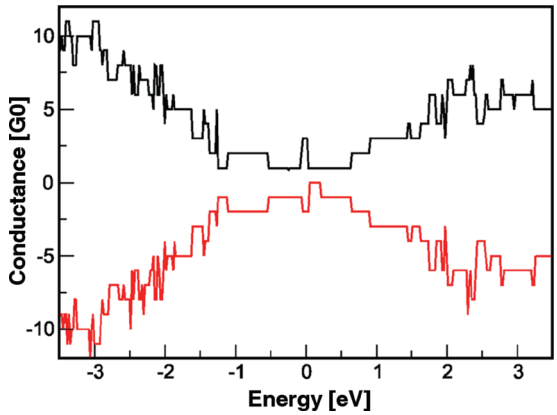

Figure 6. Quantum conductance for a typical (4,4) hybrid graphene nanoribbon. The energy gap in the minority spin for (4,4) observed in the conductance is in accordance with the band structure and the density of states (see Figures 4 and 5). The nanoribbon is spin degenerate in most of the energy spectrum, except for the region close to the Fermi level.

$N_Z = 8$, $N_A = 5$, $N_Z = 8$ HNR case). However, as the width of the armchair segment is increased, the coupling disappears, and a magnetic moment is again observed (*e.g.*, in the case of $N_Z = 3$, $N_A = 8$, $N_Z = 3$ HNR). The magnetic moments for the different HNRs calculated are listed in Table 1.

Transport Properties. Quantum conductance calculations were carried out in two different ways. First, a set of (N_A,N_Z) HNRs were considered as both leads and channels. It can be confirmed that the conductance of these HNRs is obtained straightforwardly from their density of states. The half metallicity of the (4,4) HNR is reflected in the conductance (see Figure 6), and as expected, in a small region of the energy spectrum, HNRs behave as a spin polarized conductor.

Another interesting case arises when an armchair segment is placed between two conducting zigzag nanoribbons which are used as leads (see Figure 7a). In this case, the 5−7 defects are used to join zigzag nanoribbon leads (labeled as Z) to an armchair ($N_A = 1-5$) segment. The results presented in Figure 7b demonstrate that the conductance near the Fermi level is reduced as the armchair section is increased, denoting a tunneling driven transport across the junction.

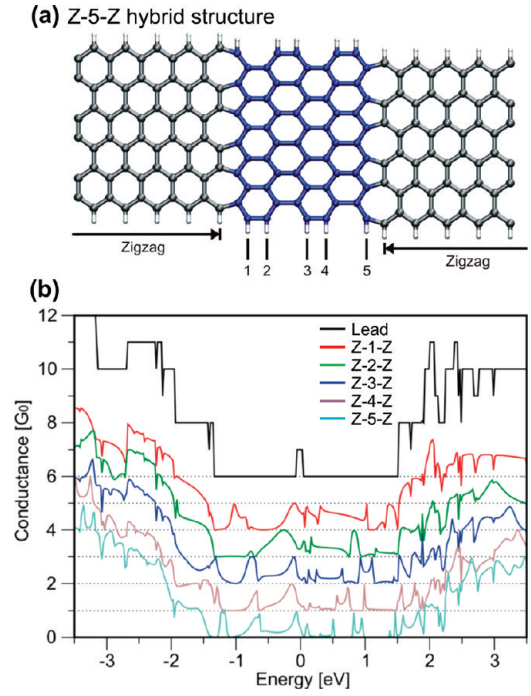

Figure 7. (a) Molecular model of a hybrid structure with zigzag leads (Z) connected by 5−7 chains to an armchair segment with $N_A = 5$ (Z-5-Z hybrid structure). (b) Quantum conductance for zigzag−armchair−zigzag devices joined by 5−7 defects. It is observed that the conductance is reduced as the armchair section is increased, revealing a tunneling driven transport.

CONCLUSIONS

Electronic and magnetic properties of hybrid graphene systems consisting of armchair-like and zigzag-like segments joined by a grain boundary formed by a linear array of 5−7-rings were fully examined using DFT calculations. The results showed that these systems exhibit electronic and magnetic properties not observed in graphene. Two-dimensional hybrid systems exhibit electronic states at the Fermi level, while one-dimensional hybrid nanoribbons (for even widths) can exhibit half metallicity without the use of an external field. Transport calculations reveal that these systems could behave as spin polarized conductors when current is applied along the HNR axis or could exhibit tunneling driven conduction if current is applied perpendicular to the HNR axis. The grain boundaries of these systems have been found experimentally, and a study of their properties is therefore important. In summary, it has been demonstrated that different arrays of structural defects (e.g. pentagons and/or heptagons) embedded in sp^2 hybridized carbon networks, could result in nanostructures exhibiting fascinating electronic properties that could be used in the development of novel electronic devices. Therefore, other possibilities of hybrid structures could be constructed and further studies still need to be carried out.

METHODOLOGY

Electronic calculations were performed using density functional theory,[38,39] within the local spin density approximation (DFT-LSDA) using the Ceperley−Alder parametrization[40] as implemented in the SIESTA code.[41] The wave functions for the valence electrons were represented by a linear combination of pseudoatomic numerical orbitals using a double-ζ polarized basis (DZP),[42] while core electrons were represented by norm-conserving Troullier−Martins pseudopotentials in the Kleynman−Bylander nonlocal form.[43,44] The real-space grid used for charge and potential integration is equivalent to a planewave cutoff energy of 150 Ry. The pseudopotentials were

constructed from 4 valence electrons for the C atoms. Periodic boundary conditions were used, and the inter-ribbon distance was kept to a minimum of 10 Å to avoid lateral interactions. Sampling of the 1D and 2D Brillouin zones was carried out with 16 × 1 × 1 and 16 × 16 × 1 Monkhorst-Pack grids, respectively. All nanoribbons were saturated with hydrogen atoms to eliminate dangling bonds and relaxed by conjugate gradient minimization until the maximum force was less than 0.04 eV/Å. Calculations using the spin polarized general gradient approximation (s-GGA) with the Perdew−Burke−Ernzerhof (PBE)[45] functional were performed in the hybrid nanoribbons in order to verify the LSDA results. Exact exchange hybrid PBE0 functional calculations were carried out using the NWChem package.[46,47]

Ab initio quantum transport properties were calculated by extracting the Hamiltonian and overlap matrices from SIESTA and using the Landauer formalism[48,49] and the surface Green's function matching method.[50,51]

Acknowledgment. The authors are grateful to D. Ramírez, G. Ramírez, and K. Gómez for technical assistance. This work was supported in part by CONACYT-México grants: 56787 (Laboratory for Nanoscience and Nanotechnology Research-LINAN), 45762 (H.T.), 60218-F1 (F.L.-U.), 45772 (M.T.), 41464-Inter American Collaboration (M.T.), 42428-Inter American Collaboration (H.T.), 2004-01-013/SALUD-CONACYT (M.T.), PUE-2004-CO29 Fondo Mixto de Puebla (M.T.), Fondo Mixto de San Luis Potosí 63001 S-3908 (M.T.), Fondo Mixto de San Luis Potosí 63072 S-3909 (H.T.), and Ph.D. Scholarship (A.R.B.-M.). V.M. and B.G.S. acknowledge work supported by the Center for Nanophase Materials Sciences (CNMS), sponsored by the Division of Scientific User Facilities, U.S. Department of Energy and by the Division of Materials Science and Engineering, U.S. Department of Energy under Contract No. DEAC05-00OR22725 with UT-Battelle, LLC at Oak Ridge National Laboratory (ORNL).

Supporting Information Available: Figure showing the band structure for (3,3), (4,4), (5,5), and (6,6) hybrid nanoribbons obtained using the PBE functional with the s-GGA approximation. This material is available free of charge *via* the Internet at http://pubs.acs.org.

REFERENCES AND NOTES

1. Novoselov, K. S.; Geim, A. K.; Morozov, S. V.; Jiang, D.; Zhang, Y.; Dubonos, S. V.; Grigorieva, I. V.; Firsov, A. A. Electric Field Effect in Atomically Thin Carbon Films. *Science* **2004**, *306*, 666–669.
2. Geim, A. K.; Novoselov, K. S. The Rise of Graphene. *Nat. Mater.* **2007**, *6*, 183–191.
3. Castro Neto, A. H.; Guinea, F.; Peres, N. M. R.; Novoselov, K. S.; Geim, A. K. The Electronic Properties of Graphene. *Rev. Mod. Phys.* **2009**, *81*, 109–154.
4. Nakada, K.; Fujita, M.; Dresselhaus, G.; Dresselhaus, M. S. Edge State in Graphene Ribbons: Nanometer Size Effect and Edge Shape Dependence. *Phys. Rev. B* **1996**, *54*, 17954.
5. Wakabayashi, K.; Fujita, M.; Ajiki, H.; Sigrist, M. Electronic and Magnetic Properties of Nanographite Ribbons. *Phys. Rev. B* **1999**, *59*, 8271.
6. Peres, N. M. R.; Guinea, F.; Castro Neto, A. H. Electronic Properties of Disordered Two-Dimensional Carbon. *Phys. Rev. B* **2006**, *73*, 125411.
7. Akhmerov, A. R.; Beenakker, C. W. J. Boundary Conditions for Dirac Fermions on a Terminated Honeycomb Lattice. *Phys. Rev. B* **2008**, *77*, 085423.
8. Ci, L.; Xu, Z.; Wang, L.; Gao, W.; Ding, F.; Kelly, K. F.; Yakobson, B. I.; Ajayan, P. M. Controlled Nanocutting of Graphene. *Nano Res.* **2008**, *1*, 116–122.
9. Datta, S. S.; Strachan, D. R.; Khamis, S. M.; Johnson, A. T. C. Crystallographic Etching of Few-Layer Graphene. *Nano Lett.* **2008**, *8*, 1912–1915.
10. Ossipov, A.; Titov, M.; Beenakker, C. W. J. Reentrance Effect in a Graphene n−p−n Junction Coupled to a Superconductor. *Phys. Rev. B* **2007**, *75*, 241401.
11. Zhang, L. M.; Fogler, M. M. Nonlinear Screening and Ballistic Transport in a Graphene p−n Junction. *Phys. Rev. Lett.* **2008**, *100*, 116804.
12. Martins, T. B.; Miwa, R. H.; da Silva, A. J. R.; Fazzio, A. Electronic and Transport Properties of Boron-Doped Graphene Nanoribbons. *Phys. Rev. Lett.* **2007**, *98*, 196803.
13. Peres, N. M. R.; Klironomos, F. D.; Tsai, S.; Santos, J. R.; Lopes dos Santos, J. M.; Castro Neto, A. H. Electron Waves in Chemically Substituted Graphene. *Europhys. Lett.* **2007**, *80*, 67007.
14. Wang, Z. F.; Shi, Q. W.; Li, Q.; Wang, X.; Hou, J. G.; Zheng, H.; Yao, Y.; Chen, J. Z-Shaped Graphene Nanoribbon Quantum Dot Device. *Appl. Phys. Lett.* **2007**, *91*, 53109.
15. Ren, H.; Li, Q.-X.; Shi, Q.-W.; Yang, J.-L. Quantum Dot Based on Z-Shaped Graphene Nanoribbon: First-Principles Study. *Chin. J. Chem. Phys.* **2007**, *20*, 489–494.
16. Wang, Z. F.; Li, Q.-X.; Shi, Q.-W.; Wang, X.; Hou, J. G.; Zheng, H.; Chen, J. Ballistic Rectification in a Z-Shaped Graphene Nanoribbon Junction. *Appl. Phys. Lett.* **2008**, *92*, 133119.
17. Chen, Y. P.; Xie, Y. E.; Zhong, J. Resonant Transport and Quantum Bound States in Z-Shaped Graphene Nanoribbons. *Phys. Lett. A* **2008**, *372*, 5928–5931.
18. Andriotis, A. N.; Menon, M. Transport Properties of Branched Graphene Nanoribbons. *Appl. Phys. Lett.* **2008**, *92*, 42115.
19. Chen, Y. P.; Xie, Y. E.; Sun, L. Z.; Zhong, J. Asymmetric Transport in Asymmetric T-Shaped Graphene Nanoribbons. *Appl. Phys. Lett.* **2008**, *93*, 92104.
20. Xu, Z.; Zheng, Q.-S.; Chen, G. Elementary Building Blocks of Graphene-Nanoribbon-Based Electronic Devices. *Appl. Phys. Lett.* **2007**, *90*, 223115.
21. Chen, Y. P.; Xie, Y. E.; Yan, X. H. Electron Transport of L-Shaped Graphene Nanoribbons. *J. Appl. Phys.* **2008**, *103*, 63711.
22. Jayasekera, T.; Mintmire, J. W. Lattice Vacancy Effects on Electron Transport in Multiterminal Graphene Nanodevices. *Int. J. Quantum Chem.* **2007**, *107*, 3071–3076.
23. Jayasekera, T.; Mintmire, J. W. Transport in Multiterminal Graphene Nanodevices. *Nanotechnology* **2007**, *18*, 424033.
24. Laakso, M. A.; Heikkila, T. T. Charge Transport in Ballistic Multiprobe Graphene Structures. *Phys. Rev. B* **2008**, *78*, 205420.
25. Wakabayashi, K.; Sigrist, M. Zero-Conductance Resonances Due to Flux States in Nanographite Ribbon Junctions. *Phys. Rev. Lett.* **2000**, *84*, 3390–3393.
26. Wakabayashi, K. Electronic Transport Properties of Nanographite Ribbon Junctions. *Phys. Rev. B* **2001**, *64*, 125428.
27. Hong, S.; Yoon, Y.; Guo, J. Meta-Semiconductor Junction of Graphene Nanoribbons. *Appl. Phys. Lett.* **2008**, *92*, 83107.
28. Yoon, Y.; Guo, J. Effect of Edge Roughness in Graphene Nanoribbon Transistors. *Appl. Phys. Lett.* **2007**, *91*, 73103.
29. Simonis, P.; Goffaux, C.; Thiry, P. A.; Biro, L. P.; Lambin, P.; Meunier, V. STM Study of a Grain Boundary in Graphite. *Surf. Sci.* **2002**, *511*, 319–322.
30. Andriotis, A. N.; Richter, E.; Menon, M. Strong Dependence of Transport Properties of Metal−Semiconductor−Metal Graphene Ribbons on Their Geometrical Features. *Appl. Phys. Lett.* **2007**, *91*, 152105.
31. Terrones, H.; Mackay, A. L. the Geometry of Hypothetical Curved Graphite Structures. *Carbon* **1992**, *30*, 1251–1260.
32. Thrower, P. A. The Study of Defects in Graphite by Transmission Electron Microscopy. *Chem. Phys. Carbon* **1969**, *5*, 217–319.
33. Rocquefelte, X.; Rignanese, G.-M.; Meunier, V.; Terrones, H.; Terrones, M.; Charlier, J.-C. How to Identify Haeckelite Structures: A Theoretical Study of Their Electronic and Vibrational Properties. *Nano Lett.* **2004**, *4*, 805–810.
34. Barone, V.; Hod, O.; Scuseria, G. E. Electronic Structure and Stability of Semiconducting Graphene Nanoribbons. *Nano Lett.* **2006**, *6*, 2748–2754.
35. Yang, L.; Park, C. H.; Son, Y. W.; Cohen, M. L.; Louie, S. G. Quasiparticle Energies and Band Gaps in Graphene Nanoribbons. *Phys. Rev. Lett.* **2007**, *99*, 186801.

36. Terrones, H.; Terrones, M.; Hernández, E.; Grobert, N.; Charlier, J.-C.; Ajayan, P. M. New Metallic Allotropes of Planar and Tubular Carbon. *Phys. Rev. Lett.* **2000**, *84*, 1716.
37. Lee, H.; Son, Y.-W.; Park, N.; Han, S.; Yu, J. Magnetic Ordering at the Edges of Graphitic Fragments: Magnetic Tail Interactions between the Edge-Localized States. *Phys. Rev. B* **2005**, *72*, 174431.
38. Hohenberg, P.; Kohn, W. Inhomogeneous Electron Gas. *Phys. Rev.* **1964**, *136*, B864.
39. Kohn, W.; Sham, L. J. Self-Consistent Equations Including Exchange and Correlation Effects. *Phys. Rev.* **1965**, *140*, A1133.
40. Ceperley, D. M.; Alder, B. J. Ground State of the Electron Gas by a Stochastic Method. *Phys. Rev. Lett.* **1980**, *45*, 566.
41. Soler, J. M.; Artacho, E.; Gale, J. D.; Garcia, A.; Junquera, J.; Ordejon, P.; Sanchez-Portal, D. The SIESTA Method for *Ab Initio* Order-N Materials Simulation. *J. Phys.: Condens. Matter* **2002**, *14*, 2745–2779.
42. Junquera, J.; Paz, O.; Sanchez-Portal, D.; Artacho, E. Numerical Atomic Orbitals for Linear-Scaling Calculations. *Phys. Rev. B* **2001**, *64*, 235111.
43. Troullier, N.; Martins, J. L. Efficient Pseudopotentials for Plane-Wave Calculations. *Phys. Rev. B* **1991**, *43*, 1993.
44. Kleinman, L.; Bylander, D. M. Efficacious Form for Model Pseudopotentials. *Phys. Rev. Lett.* **1982**, *48*, 1425.
45. Perdew, J. P.; Burke, K.; Ernzerhof, M. Generalized Gradient Approximation Made Simple. *Phys. Rev. Lett.* **1996**, *77*, 3865.
46. Adamo, C.; Barone, V. Toward Reliable Density Functional Methods without Adjustable Parameters: the PBE0 Model. *J. Chem. Phys.* **1998**, *110*, 6158–6170.
47. Bylaska, E. J. et al. NWChem, a Computational Chemistry Package for Parallel Computers, version 5.1.1 ed.; Pacific Northwest National Laboratory; Richland, WA, 2008.
48. Landauer, R. Electrical Resistance of Disordered One-Dimensional Lattices. *Philos. Mag.* **1970**, *21*, 863–867.
49. Datta, S. *Electronic Transport in Mesoscopic Systems*; Cambridge University Press: New York, 1995.
50. Nardelli, M. B. Electronic Transport in Extended Systems: Application to Carbon Nanotubes. *Phys. Rev. B* **1999**, *60*, 7828–7833.
51. Meunier, V.; Sumpter, B. G. Amphoteric Doping of Carbon Nanotubes by Encapsulation of Organic Molecules: Electronic Properties and Quantum Conductance. *J. Chem. Phys.* **2005**, *123*, 024705.